J. Ocean Univ. China (Oceanic and Coastal Sea Research)
DOI 10.1007/s11802-017-3337-1
ISSN 1672-5182, 2017 16 (4): 617-626
http://www.ouc.edu.cn/xbywb/
E-mail:xbywb@ouc.edu.cn

Model Refinement for Offshore Platforms: Experimental Study

ZHANG Min*, CHEN Zongli, and WU Yanjian

Shandong Provincial Key Laboratory of Ocean Engineering, *Ocean University of China*, *Qingdao* 266100, *P. R. China*

(Received January 3, 2017; revised May 3, 2017; accepted May 17, 2017)

Abstract Offshore jacket platforms are widely used in offshore oil and gas exploitation. Finite element models of such structures need to have many degrees of freedom (DOFs) to represent the geometrical detail of complex structures, thereby leading to incompatibility in the number of DOFs of experimental models. To bring them both to the same order while ensuring that the essential eigen-properties of the refined model match those of experimental models, an extended model refinement procedure is presented in this paper. Vibration testing of an offshore jacket platform model is performed to validate the applicability of the proposed approach. A full-order finite element model of the platform is established and then tuned to meet the measured modal properties identified from the acceleration signals. Both model reduction and modal expansion methods are investigated, as well as various scenarios of sensor arrangements. Upon completion of the refinement, the updated jacket platform model matches the natural frequencies of the measured model well.

Key words jacket platform; model refinement; model updating; model reduction; modal expansion; finite element method

1 Introduction

Steel jacket-type platforms, which are by far the most common types of offshore structures, are widely used in offshore oil and gas exploitation. These platforms are subjected to various types of environmental loading, such as wind, waves, current, and ice. As a result, structural damage caused by environmental loads accumulates continuously. To ensure the safety of offshore platforms, health monitoring and safety assessment of the structures are necessary during an offshore structure's service life.

Nowadays, structural health monitoring technology based on vibration testing allows a comprehensive evaluation of the service and health condition of the structure; such an evaluation is derived from the fact that damage to the structure might change the dynamic characteristics of the structure (Doebling *et al.*, 1998). An accurate finite element (FE) model that can replicate the measured data of real structure is necessary for evaluation. However, during vibration testing, measurements will be spatially incomplete because the number of measurement stations is generally much smaller than the number of the degrees of freedom (DOFs) in the FE model (Friswell and Mottershead, 1995; Liu and Li, 2013), especially for complex structures such as offshore platforms. When a measured model and its theoretical counterpart or two models of different sizes in general are compared, this order incompatibility presents obstacles to meaningful interpretation (Ewins, 2000). The problem can be solved by either reducing the number of DOFs in the analytical model or by expanding the number of DOFs in the measured model.

Many model reduction and modal expansion schemes have been developed, such as Guyan or static condensation (Guyan, 1965), dynamic condensation (Paz, 1984), Kidder's method (Kidder, 1973), and system equivalent reduction expansion process (SEREP) (O'Callahan *et al.*, 1989). However, the models obtained from either model reduction methods or modal expansion methods cannot represent the measured model accurately, thereby possibly causing problems in the next structural health monitoring procedure (Liu, 2011). Li *et al*. (2008) presents a refinement procedure for the reduced models. The refinement procedure involves tuning the reduced model that was obtained from one of the traditional model reduction schemes into an improved reduced model that maintains the equality of the selected modal properties of the full-order model. The mathematical kernel of the proposed model refinement technique is the cross-model cross-mode (CMCM) method (Hu *et al.*, 2007). In brief, the proposed refinement technique forms simultaneous linear equations in a matrix form, with the unknown vector being the correction factors, which are used to correct the selected stiffness and/or mass submatrices. The technique has been verified by reducing and then refining a 5-DOF classical mass-spring model into a 3-DOF generalized mass-spring model.

In this paper, the model refinement scheme is extended to combine the model refinement and updating. The ob-

* Corresponding author. Tel: 0086-532-66781672
E-mail: violet@ouc.edu.cn

jective is to first reduce the analytical model or expand the measured modal information and then refine the model to obtain an updated FE model that expresses the measured eigen-properties exactly. The method is investigated *via* modal testing of a jacket platform model. A 264-DOF jacket platform is refined into an updated model that matches the equality of identified modal parameters from the measured data. Both model reduction and modal expansion are investigated during the procedure, where the model reduction is carried out by using the static condensation (Guyan reduction) technique, while modal expansion applies SEREP. A series of scenarios with different arrangements of the accelerometers, including the number and the location, is also studied in this paper.

2 Model Refinement

The model refinement proposed by Li *et al*. (2008) aims to ensure a match between the mode shapes of the improved model match and those of the full-order model; the corresponding modal frequencies of the full-order and improved models must match as well. In the present study, the method is extended to cover both cases of model reduction and modal expansion, the aim of which is to tune the reduced/expanded model into an updated model that maintains the equality of the selected modal properties of the measured model.

In the following derivation for the model refinement procedure, to distinguish symbols for various models, the superscript ' ' is used for the reduced model, superscript '*' is used for the updated model, superscript 'm' is used for the measured model, and no superscript is used for the full-order FE model. For instance, $\boldsymbol{\Phi}$, $\boldsymbol{\Phi}'$, $\boldsymbol{\Phi}^*$ and $\boldsymbol{\Phi}^m$ represent the mode shapes of the full-order, reduced, updated, and measured models, respectively. As the full-order model is usually formed by an FE procedure, the measured model is usually obtained by modal identification from modal testing. The corresponding measured mode shapes $\boldsymbol{\Phi}_j^m$ and modal frequencies ω_j^m $(j=1,\cdots,N_s)$ are identified from the measured data, in which N_s is the number of identified modes. The reduced model is obtained from the full-order model *via* a traditional model reduction scheme, and the expanded mode shape data are obtained through the modal expansion method based on identified modal shapes from measured response signals. The updated model is tuned from the reduced model/full-order model through the refinement technique presented below.

2.1 Model Refinement for Model Reduction

In the reduction procedure, the stiffness and mass matrices of the reduced model, $\boldsymbol{K}'$ and $\boldsymbol{M}'$, are obtained by using one of the traditional model reduction methods. Then, the corresponding mode shapes $\boldsymbol{\Phi}_i'$ and modal frequencies ω_i' $(i=1,\cdots,N_t)$, where N_t is the number of modes for the reduced model, can be computed accordingly. The refinement procedure aims to refine the stiffness and mass matrices from $\boldsymbol{K}'$ and $\boldsymbol{M}'$ to $\boldsymbol{K}^*$ and $\boldsymbol{M}^*$, as several $\boldsymbol{\Phi}_j^*$ and ω_j^* associated with $\boldsymbol{K}^*$ and $\boldsymbol{M}^*$ must match well with the related $\boldsymbol{\Phi}_j^m$ and ω_j^m.

The stiffness matrix $\boldsymbol{K}^*$ of the updated reduced model is a correction of $\boldsymbol{K}'$ as follows:

$$\boldsymbol{K}^* = \boldsymbol{K}' + \sum_{n=1}^{N_K} \alpha_n \boldsymbol{K}_n' , \tag{1}$$

where any individual $\boldsymbol{K}_n'$ is a pre-selected stiffness submatrix of the reduced model; N_K is the number of stiffness correction terms; and α_n is the unknown stiffness correction factors to be determined. The corresponding expression for the mass matrix $\boldsymbol{M}^*$ is written as

$$\boldsymbol{M}^* = \boldsymbol{M}' + \sum_{n=1}^{N_M} \beta_n \boldsymbol{M}_n' , \tag{2}$$

where the individual $\boldsymbol{M}_n'$ is a pre-selected mass sub-matrix of the reduced model; N_M is the number of correction coefficients for the mass matrix; and β_n is the mass correction coefficients to be determined.

For the jth eigenvalue λ_j^* and eigenvector $\boldsymbol{\Phi}_j^*$ associated with $\boldsymbol{K}^*$ and $\boldsymbol{M}^*$, the following is written:

$$\boldsymbol{K}^* \boldsymbol{\Phi}_j^* = \lambda_j^* \boldsymbol{M}^* \boldsymbol{\Phi}_j^* . \tag{3}$$

In the following development, λ_j^* and $\boldsymbol{\Phi}_j^*$ should be treated as known quantities available from the measured model, that is, $\lambda_j^* = \lambda_j^m$ and $\boldsymbol{\Phi}_j^* = \boldsymbol{\Phi}_j^m$.

Denoting superscript 'T' as the transpose operator and premultiplying Eq. (3) by $(\boldsymbol{\Phi}_i')^{\mathrm{T}}$ yields

$$(\boldsymbol{\Phi}_i')^{\mathrm{T}} \boldsymbol{K}^* \boldsymbol{\Phi}_j^* = \lambda_j^* (\boldsymbol{\Phi}_i')^{\mathrm{T}} \boldsymbol{M}^* \boldsymbol{\Phi}_j^* . \tag{4}$$

Substituting Eqs. (1) and (2) into the above equation leads to

$$\boldsymbol{K}_{ij}^{\dagger} + \sum_{n=1}^{N_K} \alpha_n \boldsymbol{K}_{n,ij}^{\dagger} = \lambda_j^* (\boldsymbol{M}_{ij}^{\square} + \sum_{n=1}^{N_K} \beta_n \boldsymbol{M}_{n,ij}) , \tag{5}$$

where

$$\boldsymbol{K}_{ij}^{\dagger} = (\boldsymbol{\Phi}_i')^{\mathrm{T}} \boldsymbol{K} \boldsymbol{\Phi}_j^* , \quad \boldsymbol{K}_{n,ij}^{\dagger} = (\boldsymbol{\Phi}_i')^{\mathrm{T}} \boldsymbol{K}_n \boldsymbol{\Phi}_j^* ,$$

$$\boldsymbol{M}_{ij}^{\dagger} = (\boldsymbol{\Phi}_i')^{\mathrm{T}} \boldsymbol{M} \boldsymbol{\Phi}_j^* , \quad \boldsymbol{M}_{n,ij}^{\dagger} = (\boldsymbol{\Phi}_i')^{\mathrm{T}} \boldsymbol{M}_n \boldsymbol{\Phi}_j^* .$$

For clarity, symbols with superscript '†' throughout this paper are 'cross' terms calculated from both reduced and updated reduced models. Using a new index m to replace ij and rearranging Eq. (5) yields

$$\sum_{n=1}^{N_K} \alpha_n \boldsymbol{K}_{n,m}^{\dagger} + \sum_{n=1}^{N_M} \beta_n (-\lambda_j^* \boldsymbol{M}_{n,m}^{\square}) = \boldsymbol{f}_m , \tag{6}$$

where

$$\boldsymbol{f}_m^{\dagger} = \lambda_j^* \boldsymbol{M}_m^{\square} - \boldsymbol{K}_m .$$

When N_i modes are taken from the reduced model and N_j modes are taken from the measured model, a total of $N_m = N_i \times N_j$ equations can be formed from Eq. (6). Those equations are named CMCM equations because they are formed by crossing over two models, namely, the reduced and the updated reduced models, as well as various modes.

Expressing Eq. (6) in a matrix form one obtains

$$\boldsymbol{K}^{\dagger}\boldsymbol{\alpha}+\boldsymbol{M}^{\dagger}\boldsymbol{\beta}=\boldsymbol{f}^{\dagger}, \tag{7}$$

in which $\boldsymbol{K}^{\dagger}$ and $\boldsymbol{M}^{\dagger}$ are N_m-by-N_K and N_m-by-N_M matrix, respectively; $\boldsymbol{\alpha}$ and $\boldsymbol{\beta}$ are column vectors of size N_K and N_M, respectively; and $\boldsymbol{f}^{\dagger}$ is a column vector of size N_m. Furthermore, Eq. (7) can be rewritten as

$$\boldsymbol{G}^{\dagger}\boldsymbol{\gamma}=\boldsymbol{f}^{\dagger}, \tag{8}$$

where

$$\boldsymbol{G}^{\dagger}=[\boldsymbol{K}^{\dagger}\boldsymbol{M}^{\dagger}], \text{ and } \boldsymbol{\gamma}=\begin{Bmatrix}\boldsymbol{\alpha}\\ \boldsymbol{\beta}\end{Bmatrix}.$$

Analytically, $\boldsymbol{\gamma}$ in Eq. (8) can be solved by using a standard inverse operation, $\boldsymbol{\gamma}=\boldsymbol{f}^{\dagger}\boldsymbol{G}^{\dagger-1}$, if $G^{\dagger}$ is a non-singular square matrix. For a non-square matrix $\boldsymbol{G}^{\dagger}$ where the number of equations does not equal the number of unknowns, the equivalent operator is the pseudo-inverse. If $\boldsymbol{G}^{\dagger}$ has more rows than columns, then, for an overdetermined case where more equations exist than unknowns, the pseudo-inverse is defined as

$$\boldsymbol{G}^{\dagger\#}=(\boldsymbol{G}^{\square}\ \boldsymbol{G}\ )^{-}\ \boldsymbol{G}\quad, \tag{9}$$

for non-singular($\boldsymbol{G}^{\dagger\mathrm{T}}\boldsymbol{G}^{\dagger}$). The resultant solution, $\boldsymbol{\gamma}=\boldsymbol{f}^{\dagger}\boldsymbol{G}^{\dagger\#}$ is optimal in a least-squares sense.

2.2 Model Refinement for Modal Expansion

For the modal expansion procedure, the measured mode shapes $\boldsymbol{\Phi}^{m}$ are extended to be $\boldsymbol{\Phi}_e^{m}$ by applying one of the traditional modal expansion schemes to meet the number of DOFs in the analytical full-order model. The objective is to ensure a match between the mode shapes of the updated model and the expanded mode shapes of the measured model, as well as the corresponding natural frequencies, *i.e.*, attempting to make $\boldsymbol{\Phi}^{*}=\boldsymbol{\Phi}_e^{m}$ and $\lambda_j^{*}=\lambda_j^{m}$ by refining the selected mass and stiffness matrices of the full-order model. The entire procedure is similar to the above model reduction.

The stiffness matrix and mass matrix of the updated model, $\boldsymbol{K}^{*}$ and $\boldsymbol{M}^{*}$, can also be expressed as corrections of the full-order model

$$\boldsymbol{K}^{*}=\boldsymbol{K}+\sum_{n=1}^{N_K}\alpha_n\boldsymbol{K}_n, \tag{10}$$

$$\boldsymbol{M}^{*}=\boldsymbol{M}+\sum_{n=1}^{N_M}\beta_n\boldsymbol{M}_n, \tag{11}$$

where $\boldsymbol{K}_n$ and $\boldsymbol{M}_n$ are the pre-selected stiffness sub-matrix and the mass sub-matrix of the full-order model, respectively; and α_n and β_n are correction coefficients to be determined.

Premultiplying Eq. (3) by $(\boldsymbol{\Phi}_i)^{\mathrm{T}}$ yields an equation with a similar form as Eq. (4)

$$(\boldsymbol{\Phi}_i)^{\mathrm{T}}\boldsymbol{K}^{*}\boldsymbol{\Phi}_j^{*}=\lambda_j^{*}(\boldsymbol{\Phi}_i)^{\mathrm{T}}\boldsymbol{M}^{*}\boldsymbol{\Phi}_j^{*}. \tag{12}$$

Substituting Eqs. (10) and (11) into the above equation and rearranging yields

$$\sum_{n=1}^{N_K}\alpha_n\boldsymbol{K}_{n,m}^{\dagger}+\sum_{n=1}^{N_M}\beta_n(-\lambda_j^{*}\boldsymbol{M}_{n,m}^{\square})=\boldsymbol{f}_m, \tag{13}$$

where

$$\boldsymbol{K}_{ij}^{\dagger}=(\boldsymbol{\Phi}_i)^{\mathrm{T}}\boldsymbol{K}\boldsymbol{\Phi}_j^{*},\ \boldsymbol{K}_{n,ij}^{\dagger}=(\boldsymbol{\Phi}_i)^{\mathrm{T}}\boldsymbol{K}_n\boldsymbol{\Phi}_j^{*},$$

$$\boldsymbol{M}_{ij}^{\dagger}=(\boldsymbol{\Phi}_i)^{\mathrm{T}}\boldsymbol{M}\boldsymbol{\Phi}_j^{*},\ \boldsymbol{M}_{n,ij}^{\dagger}=(\boldsymbol{\Phi}_i)^{\mathrm{T}}\boldsymbol{M}_n\boldsymbol{\Phi}_j^{*},$$

$$\boldsymbol{f}_m^{\dagger}=\lambda_j^{*}\boldsymbol{M}_m^{\square}-\boldsymbol{K}_m.$$

Those equations are also CMCM equations, which are formed by crossing over full-order and updated models, as well as various models.

The CMCM equations can also be expressed in a matrix form as Eq. (7), and the same solution procedure can be used to calculate the correction factors α and β as mentioned above.

3 Experimental Study

3.1 Model Description

In the vibration testing experiment, a scaled steel tube frame physical model is applied, the prototype of which is an offshore jacket platform in service in Bohai Bay, China. The model consists of four stories and four legs and other cross-bracings that are welded through steel. The top is welded with a homogeneous steel plate to simulate the topside of the platform. The height of the model is 1.52 m, and the dimension of the base is 0.77 m (*x*-direction) × 0.54 m (*y*-direction). The sectional dimensions of the members are as follows: the legs are 20 mm in diameter and 2 mm thick, the braces are 10 mm in diameter and 2 mm thick, and the deck is 20 mm thick.

The corresponding FE model is also established. A total of 44 unconstrained nodes are present in this FE model; each node has 6 degrees of freedom. Thus, this FE full-order model is a 264-DOF 3D model. The analytical and measured platform models are shown in Fig.1. The natural frequencies of the first three modes of the FE model and the corresponding mode shapes are shown in Fig.2.

3.2 Modal Testing

In this experiment, the test model was fixed on a shaker by the flanges at the ends of four legs. A total of eight unidirectional accelerometers and 18 triaxial accelerometers are placed for signal acquisition (shown in Fig.3). Thus, the number of channels, *i.e.*, the number of measured DOFs, totals 62. Impulse excitation was generated by a rubber hammer, and the acceleration vibration response data of the structure were collected. Throughout the experiment, the data sampling frequency was 200 Hz. The time histories of measured acceleration signals in three directions of one node are shown in Fig.4.

3.3 Modal Parameter Identification

Modal parameter identification was performed by us-

ing polyreference complex exponential (PRCE) method (Ewins, 2000; Maia *et al.*, 1997). PRCE is a well-known time domain method used for experimental modal analysis. It was conceived to be a major step forward because multiple references allow repeated roots to be estimated, and in general, PRCE efficiently uncouples closely coupled modes (Hu *et al.*, 2012).

When implementing PRCE, the model order needs to be determined. In practice, applying the PRCE algorithm for experimental data often requires the model order to be overspecified. To eliminate spurious numerical modes, the stability diagram is applied in this paper. When producing a stability diagram, the poles that correspond to a certain model order are compared with the poles of a one-order-lower model (Hu *et al.*, 2010; Peeters, 2000). If the modal frequency and the damping ratio differences are within preset limits, then the pole is labeled as stable. The stability diagram obtained from implementing PRCE by choosing the model orders ranging from 10 to 50 is shown

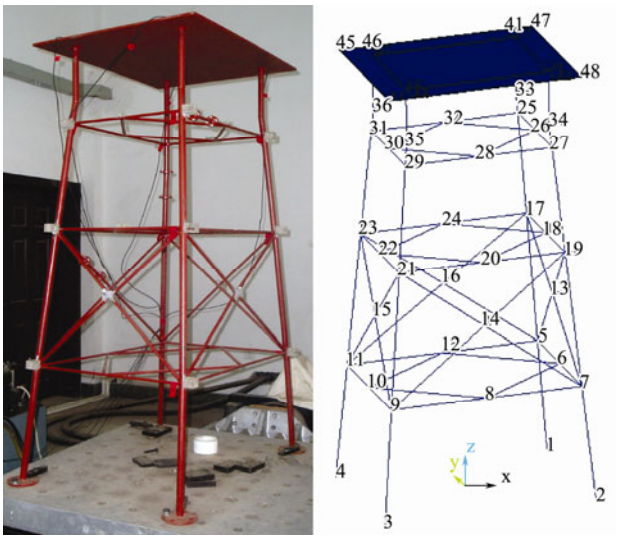

Fig.1 Physical (left) and FE model (right) of the offshore platform.

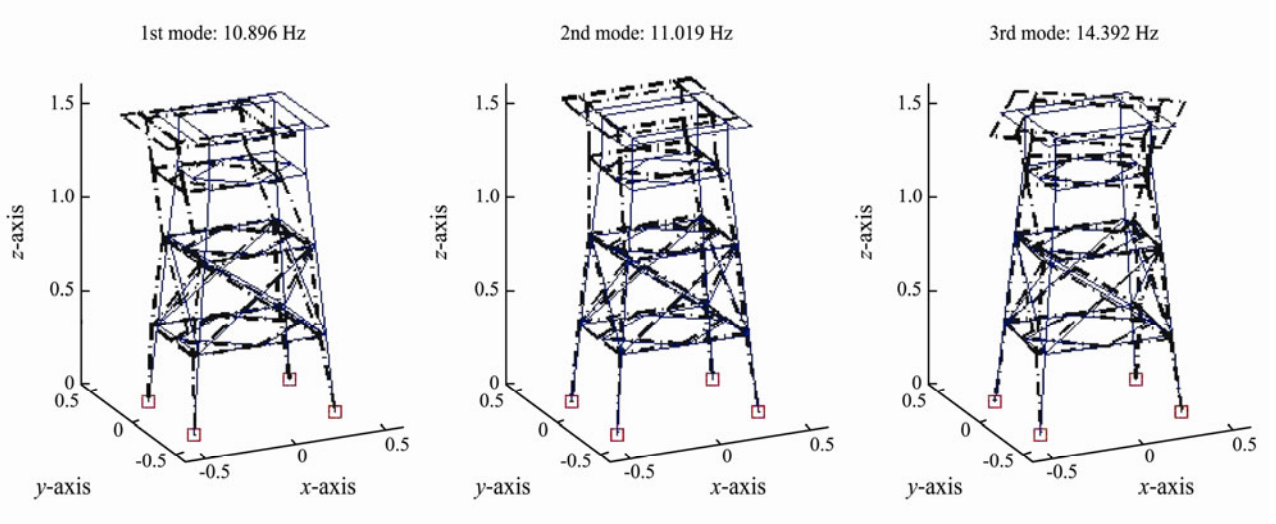

Fig.2 First three modes of the FE model.

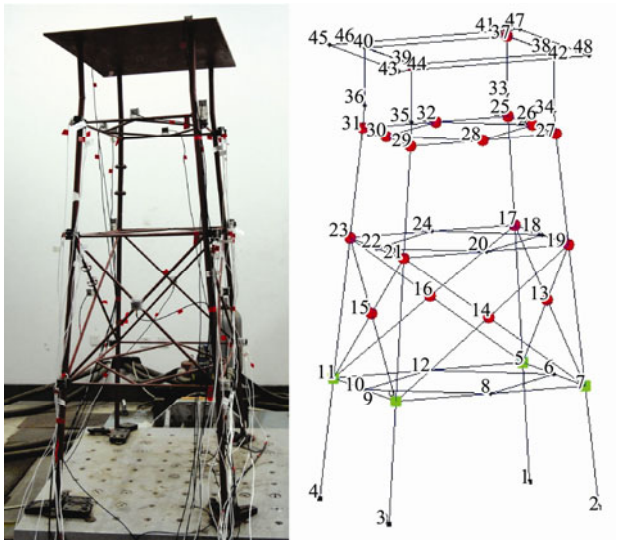

Fig.3 Sensor arrangement (red dots: triaxial accelerometer; green square: two unidirectional accelerometers in the *x* and *y* directions, respectively).

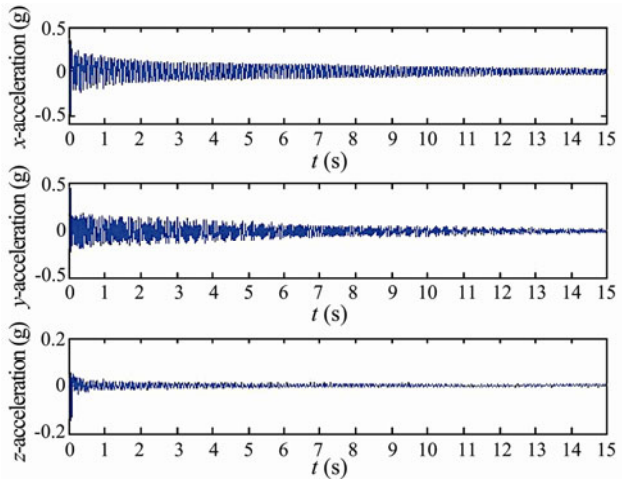

Fig.4 Measured response acceleration signals of three directions on one node.

in Fig.5, in which poles are labeled as stable when they are within the limitations of 1% difference for the natural

frequency and 5% for the damping ratio (Hu *et al.*, 2012), that is,

$$\frac{\left|f^{(n)}-f^{(n+1)}\right|}{f^{(n)}}<1\%, \tag{14}$$

$$\frac{\left|\xi^{(n)}-\xi^{(n+1)}\right|}{\xi^{(n)}}<5\%. \tag{15}$$

In this figure, the poles that meet the preset stability standard are labeled as ‘ * ’ and are labeled ‘o’ otherwise. On the basis of the power spectrum density diagram of the measured signal from the output-reference channel and according to the frequency range of the FE model, the stability diagram has consistent frequency estimates near three system frequencies that extend from lower-order to higher-order models. The first three identified modal parameters are shown in Fig.6. A comparison among the first three natural frequencies of the FE model and the testing model indicates differences, especially in the second and third modes (Table 1). The objective is to refine the FE full-order model through both model reduction and modal expansion to obtain an updated model that replicates the measured model.

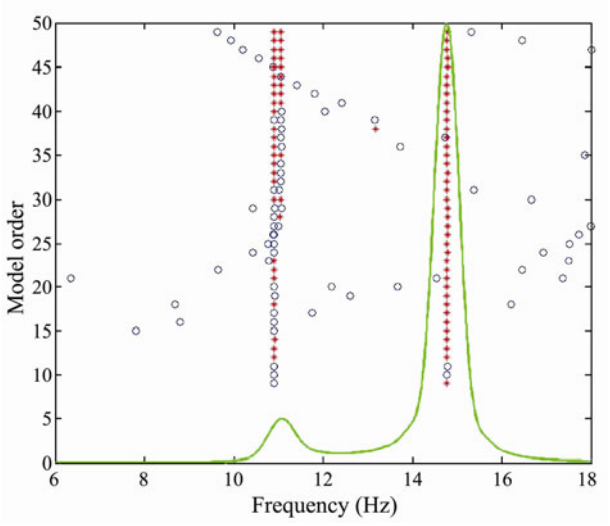

Fig.5 Stability diagram obtained from implementing PRCE (‘*’: stable; ‘o’: unstable).

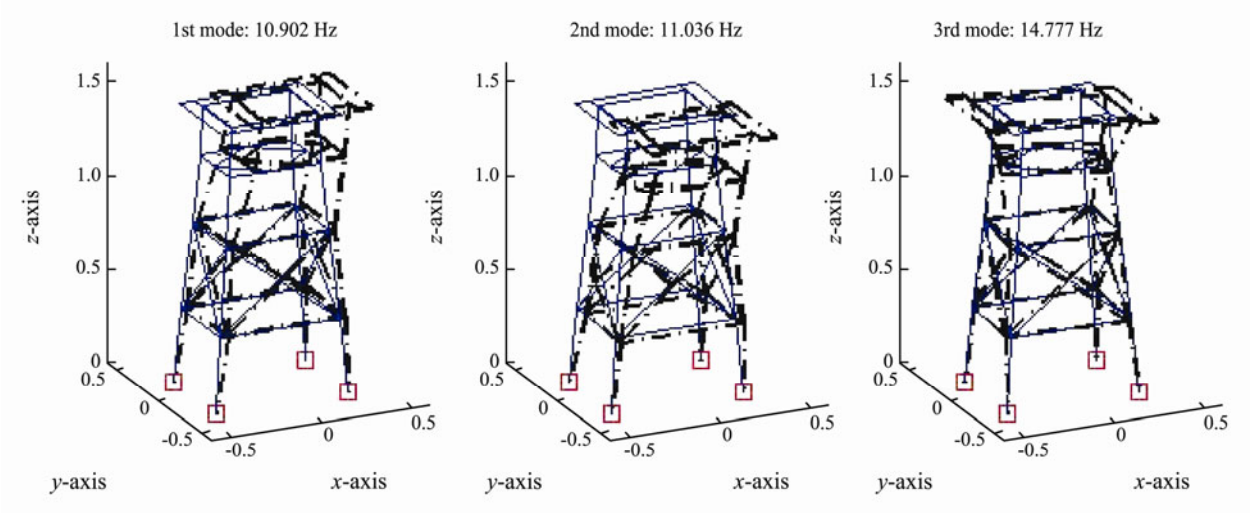

Fig.6 First three identified modes of the test model.

Table 1 Frequencies and MAC values for the reduced model

Mode	Full order model		Reduced model (Guyan reduction)		Measured model
	Freq. (Hz)	MAC	Freq. (Hz)	MAC	Freq. (Hz)
1	10.896	0.9424	10.897	0.9424	10.902
2	11.019	0.9256	11.019	0.9256	11.036
3	14.392	0.9850	14.393	0.9850	14.777

3.4 Model Refinement of Jacket Platform Model Through Model Reduction

3.4.1 Model reduction of the full-order model

When performing model reduction, the master DOFs can be taken as the locations where the accelerometers are placed, of which the total number is 62. Thus, the full-order model can be reduced from 264 DOFs to 62 DOFs on the basis of the model reduction scheme by applying Guyan (static) reduction.

Static reduction is the most widely adopted model reduction scheme and was introduced by Guyan (Friswell and Mottershead, 1995; Guyan, 1965). This technique partitions mass and stiffness matrices and the displacement vector into a set of master and slave DOFs.

$$\begin{bmatrix}\boldsymbol{M}_m & \boldsymbol{M}_{ms}\\ \boldsymbol{M}_{sm} & \boldsymbol{M}_s\end{bmatrix}\begin{Bmatrix}\ddot{\boldsymbol{x}}_m\\ \ddot{\boldsymbol{x}}_s\end{Bmatrix}+\begin{bmatrix}\boldsymbol{K}_m & \boldsymbol{K}_{ms}\\ \boldsymbol{K}_{sm} & \boldsymbol{K}_s\end{bmatrix}\begin{Bmatrix}\boldsymbol{x}_m\\ \boldsymbol{x}_s\end{Bmatrix}=\begin{Bmatrix}0\\ 0\end{Bmatrix}. \tag{16}$$

The subscripts m and s denote the master and slave coordinates, respectively. The inertia terms for the second set of equations may be neglected to eliminate the slave DOFs, thereby obtaining

$$\begin{Bmatrix}\boldsymbol{x}_m\\ \boldsymbol{x}_s\end{Bmatrix}=\boldsymbol{T}_G\boldsymbol{X}_m, \tag{17}$$

where

$$\boldsymbol{T}_G = \begin{bmatrix} \boldsymbol{I} \\ -\boldsymbol{K}_s^{-1}\boldsymbol{K}_{sm} \end{bmatrix}, \tag{18}$$

is the Guyan transformation matrix. The reduced mass and stiffness matrices are then given by

$$\boldsymbol{M}_G = \boldsymbol{T}_G^{\mathrm{T}}\boldsymbol{M}\boldsymbol{T}_G\,, \tag{19}$$

and

$$\boldsymbol{M}_G = \boldsymbol{T}_G^{\mathrm{T}}\boldsymbol{M}\boldsymbol{T}_G\,, \tag{20}$$

where $\boldsymbol{M}_G$ and $\boldsymbol{K}_G$ denote the reduced mass and stiffness matrices associated with the Guyan reduction scheme, respectively.

The resultant frequencies of the reduced models and the modal assurance criterion (MAC) values between the reduced and measured models are shown in Table 1, where the MAC value between modes $\boldsymbol{\Phi}_i$ and $\boldsymbol{\Phi}_j$ is defined as

$$\mathrm{MAC}(\boldsymbol{\Phi}_i, \boldsymbol{\Phi}_j) = \frac{\left|\boldsymbol{\Phi}_i^{\mathrm{T}}\boldsymbol{\Phi}_j\right|^2}{(\boldsymbol{\Phi}_i^{\mathrm{T}}\boldsymbol{\Phi}_i)(\boldsymbol{\Phi}_j^{\mathrm{T}}\boldsymbol{\Phi}_j)}\,, \tag{21}$$

where $\left|\boldsymbol{\Phi}_i\right|$ denotes the length (norm) of $\boldsymbol{\Phi}_i$. The MAC value is always between 0 and 1, and a value of 1 indicates that the two modes have the same shape. Table 1 indicates that for the lower modes, Guyan reduction agrees well with the modal properties of the full system. This finding also indicates discrepancies between the reduced model and the measured model. The next task is to refine the reduced model to meet the modal properties of the measured model.

3.4.2 Selection of updating elements based on sensitivity studies

In applying the model refinement scheme, one starts numerically with $\boldsymbol{K}' = \boldsymbol{K}_G$ and $\boldsymbol{M}' = \boldsymbol{M}_G$. The next issue is how submatrices $\boldsymbol{K}_n'$ and $\boldsymbol{M}_n'$ should be selected. An easy step is to consider choosing the element stiffness and mass matrices of each element as the updating submatrices. This platform FE model contains 77 elements, and including all the 77 elements in the refinement procedures is not necessary and efficient for calculation. The updating element candidates should be selected or optimized prior to the model refinement, which can be solved by locating the modeling error.

In this experiment, damages to the structure are simulated by reducing the diameter/thickness of the members. This reduction is achieved by replacing one segment of the whole element by different replacements, as shown in Fig.7. The replacements and the structure members are connected by flanges. Thus, the damage simulation may influence the stiffness of the elements, which may result in the differences between the analytical and measured models. As a result, elements 25, 51, and 60, where the damages are located (Fig.8), should be considered the updating element candidates. Moreover, the mass of the steel plate on the top may differ between the analytical and measured models because of the inaccurate fabrication procedure. The stiffness matrices of elements 25, 51, and 60 and the mass matrices of deck elements 73–77 can be selected as the updating candidates.

Fig.7 Replacements for damage simulation.

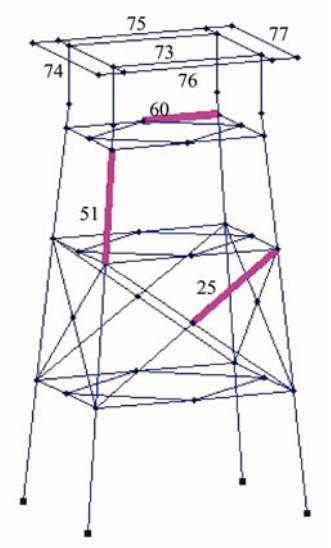

Fig. 8 Locations of updating elements.

After choosing the updating candidates, the next step is to check the sensitivity of the updating parameters to the first three modes. The sensitivity can be calculated by using Eq. (22) (Rade and Lallement, 1998) and is equal to the modal kinetic energy and modal strain energy of the element.

$$\begin{cases} \boldsymbol{S}_j^k = \dfrac{1}{m}\displaystyle\sum_{i=1}^{m}\boldsymbol{MSE}_{ij} = \dfrac{1}{m}\displaystyle\sum_{i=1}^{m}\boldsymbol{\Phi}_i^{\mathrm{T}}\boldsymbol{K}_j\boldsymbol{\Phi}_i \\ \boldsymbol{S}_j^m = \dfrac{1}{m}\displaystyle\sum_{i=1}^{m}\boldsymbol{MKE}_{ij} = \dfrac{1}{m}\displaystyle\sum_{i=1}^{m}\lambda_i\boldsymbol{\Phi}_i^{\mathrm{T}}\boldsymbol{M}_j\boldsymbol{\Phi}_i \end{cases}. \tag{22}$$

The sensitivity results are shown in Fig.9. The figure shows that the deck elements (elements 73–77) have higher sensitivity than the pipe elements. The pipe elements and deck elements cannot be updated simultaneously because of the significant discrepancy. Then, according to the values of sensitivity, the candidate updating elements are divided into two groups, namely, group 1: elements 51 and 60, and group 2: elements 73–77. Element 25 is eliminated from the candidates because it has

the lowest sensitivity. Moreover, as shown in Fig.8, element 25 is a brace member in the second floor, where the stiffness is larger. The damage simulation of this element will not considerably change the stiffness of this part; thus, it does not influence the stiffness of the entire structure.

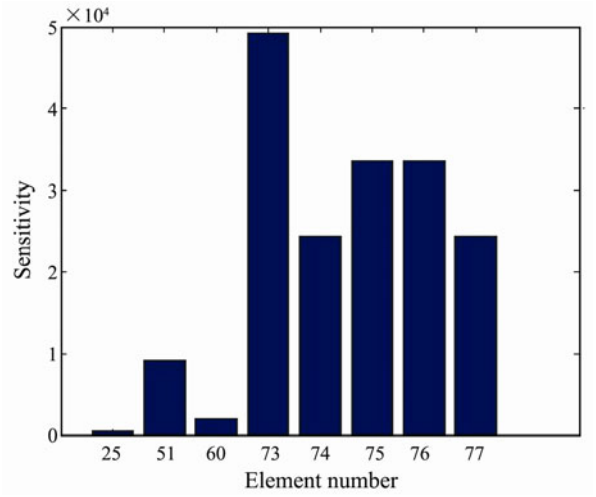

Fig.9 Sensitivity of the updating element candidates to the first three modes.

From the analysis above, the submatrices $\boldsymbol{K}_n'$ and $\boldsymbol{M}_n'$ can be selected as

$$\boldsymbol{K}_1' = \boldsymbol{T}_G^{\mathrm{T}} \boldsymbol{K}_{51} \boldsymbol{T}_G,\ \boldsymbol{K}_2' = \boldsymbol{T}_G^{\mathrm{T}} \boldsymbol{K}_{60} \boldsymbol{T}_G,$$

$$\boldsymbol{M}_1' = \boldsymbol{T}_G^{\mathrm{T}} \boldsymbol{M}_{73} \boldsymbol{T}_G,\ \boldsymbol{M}_2' = \boldsymbol{T}_G^{\mathrm{T}} \boldsymbol{M}_{74} \boldsymbol{T}_G,\ \boldsymbol{M}_3' = T_G^{\mathrm{T}} \boldsymbol{M}_{75} \boldsymbol{T}_G,$$

$$\boldsymbol{M}_4' = \boldsymbol{T}_G^{\mathrm{T}} \boldsymbol{M}_{76} \boldsymbol{T}_G,\ \boldsymbol{M}_5' = \boldsymbol{T}_G^{\mathrm{T}} \boldsymbol{M}_{77} \boldsymbol{T}_G,$$

where $\boldsymbol{T}_G$ is the Guyan transformation matrix; $\boldsymbol{K}_{51}$ and $\boldsymbol{K}_{60}$ are the stiffness matrices of elements 51 and 60, respectively; and $\boldsymbol{M}_{73}$ to $\boldsymbol{M}_{77}$ are the mass matrices of elements 73 to 77. The refinement procedure is performed below.

3.4.3 Refinement of reduced model

a) Target modes: the first and second modes ($\boldsymbol{K}_1'$ and $\boldsymbol{K}_2'$)

In applying the CMCM method, five modes of the reduced model and the first two modes of the measured model are integrated into Eq. (6) to form 10 CMCM equations. The resultant stiffness correction factors are α_1= 0.059, α_2=−0.089, which means that the stiffness of element 51 should increase by 5.9% and that of element 60 should decrease by 8.9%. After refinement, the resultant modal frequencies match better with those of the first two modes of the measured model (Table 2). However, the MAC values did not improve sufficiently because the updated elements are too few to have a significant influence on the mode shapes. Therefore, only the natural frequencies are listed for comparison.

b) Target modes: the first three modes ($\boldsymbol{M}_1' - \boldsymbol{M}_5'$)

Following the same procedure in the above step, five modes of the reduced model and the first three modes of the measured model are employed to form 15 CMCM equations. The resultant mass correction factors are β_1= 0.10585, β_2=−0.14336, β_3=−0.035682, β_4=−0.032243, and β_5=−0.14162. For the symmetrical location of the updating element $\boldsymbol{M}_2'$ and $\boldsymbol{M}_5'$; $\boldsymbol{M}_3'$ and $\boldsymbol{M}_4'$, symmetrical values of updating parameters should be obtained. After refinement, the three natural frequencies agree well with those of the measured model (Table 3).

Table 2 Frequencies and MAC values for the improved reduced model (after step 1)

Mode	Reduced model (Guyan reduction)		Updated reduced model (after step 1)		Measured model
	Freq. (Hz)	MAC	Freq. (Hz)	MAC	Freq. (Hz)
1	10.897	0.9424	10.9	0.9404	10.902
2	11.019	0.9256	11.033	0.9254	11.036
3	14.393	0.9850	14.411	0.9850	14.777

Table 3 Frequencies and MAC values for the improved reduced model

Mode	Frequency (Hz)			
	Reduced model (Guyan reduction)	Updated reduced model (after step 1)	Updated reduced model (after step 2)	Measured model
1	10.897	10.9	10.903	10.902
2	11.019	11.033	11.034	11.036
3	14.393	14.411	14.777	14.777

3.4.4 Model refinement for limited sensor arrangement

The sensors can be placed anywhere on the structure for lab experiments. However, for the real offshore platform structure, the numbers and locations of the sensors are limited because of the hostile service environment. Placing sensors underwater is technically and economically prohibitive in an on-site vibration testing or online monitoring system. In the following section, model refinement for the limited sensor arrangement case is investigated to meet practical engineering requirements.

a) Sensor number: 14

If the number of sensors is reduced to 14, then the measured DOFs number 42; the arrangement is shown in Fig.10. The reduced model is also obtained by using Guyan reduction. A comparison between the full-order and the reduced models is shown in Table 4. Following the same procedure above, the following correction factors are obtained: α_1=0.08358, α_2=−0.1211, and β_1= 0.10574, β_2=−0.14291, β_3=−0.0358, β_4=−0.0328, and β_5= −0.13565. The natural frequencies of the first three modes of the updated reduced model also match the measured model perfectly in this case, as shown in Table 4.

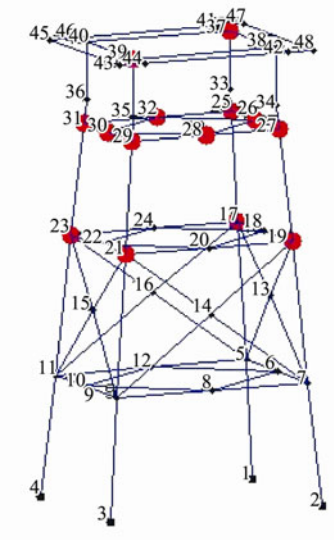

Fig.10 Arrangement of 14 sensors (red dots: triaxial accelerometer).

b) Sensor number: 10

In this case, all the sensors are placed above the water. The measured DOFs are 30, and the arrangement is shown in Fig.11. Following the same procedure above, the following correction factors are obtained: α_1=0.1104, α_2=−0.2206, β_1=0.1020, β_2=−0.1389, β_3=−0.034, β_4=−0.033, and β_5=−0.1313. The natural frequencies of the first three modes of the updated reduced model are shown in Table 5. The table shows that as the number of sensors is reduced, the discrepancy increases between the modal properties of updated reduced model and measured model. An iteration procedure is needed to obtain a more accurate result.

In this iteration procedure, first, the updated reduced model in the last step is taken as the reduced model in the next step, *i.e.*, $\boldsymbol{K}^{(n+1)}=\boldsymbol{K}^{*(n)}$ and $\boldsymbol{M}^{(n+1)}=\boldsymbol{M}^{*(n)}$. Then, the model refinement method is applied to calculate the stiffness and mass matrix correction factors α and β, as well as obtain the new updated reduced model, $\boldsymbol{K}^*$ and $\boldsymbol{M}^*$. The above procedure is repeated until the correction factors converge. The obtained correction factors are α_1=0.4847, α_2=−0.0947, β_1=0.1721, β_2=0.0528, β_3=−0.1989, β_4=−0.0446, and β_5=−0.0656. Table 6 shows the final frequencies and MAC values of the updated reduced model. The natural frequencies of the updated reduced model match the measured model better than the reduced model can after iteration.

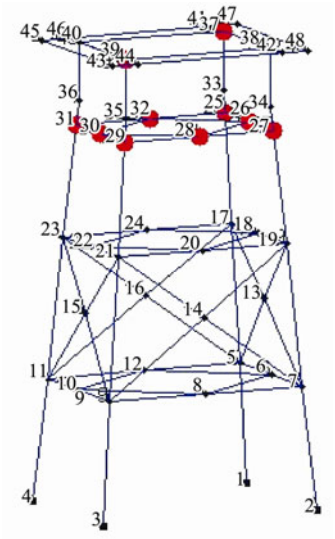

Fig.11 Arrangement of 10 sensors (red dots: triaxial accelerometer).

Table 4 Frequencies and MAC values for the improved reduced model (14 sensors)

Mode	Frequency (Hz)			
	Reduced model (Guyan reduction)	Updated reduced model (after step 1)	Updated reduced model (after step 2)	Measured model
1	10.897	10.902	10.902	10.902
2	11.019	11.036	11.036	11.036
3	14.393	14.419	14.777	14.777

Table 5 Frequencies and MAC values for the improved reduced model (10 sensors)

Mode	Frequency (Hz)			
	Reduced model (Guyan reduction)	Updated reduced model (after step 1)	Updated reduced model (after step 2)	Measured model
1	10.899	10.899	10.895	10.902
2	11.022	11.048	11.043	11.035
3	14.399	14.432	14.777	14.777

Table 6 Frequencies and MAC values for the improved reduced model after iteration (10 sensors)

Mode	Frequency (Hz)			
	Full-order model	Reduced model (Guyan reduction)	Updated reduced model (after interaction)	Measured model
1	10.896	10.899	10.902	10.902
2	11.019	11.022	11.035	11.034
3	14.392	14.399	14.777	14.777

3.5 Model Refinement Through Modal Expansion

In this section, instead of model reduction, the incomplete measured modal shapes are expanded to full-order modal properties by using modal expansion methods. The master DOFs are still the location in which a total of 62 accelerometers are placed. Three traditional model expansion methods, namely, Guyan expansion, Kidder's method, and SEREP, are used to expand 62 DOFs to 264 full-order DOFs.

The resultant MAC values between the expanded and analytical mode shapes are shown in Table 7. Guyan expansion and Kidder's method obtained similar results, whereas SEREP performed better, obtaining MAC values of nearly 1. This result is reasonable because SEREP uses the analytical model for interpolation, thereby ensuring that the expanded mode shapes correlate well with the analytical model (Ewins, 2000). The expanded mode shape from SEREP is then selected as the initial-order measured mode shape. The next task is to update the FE model to meet the expanded modal properties.

The updating submatrices $\boldsymbol{K}_n$ and $\boldsymbol{M}_n$ are selected as

$$\boldsymbol{K}_1=\boldsymbol{K}_{51},\ \boldsymbol{K}_2=\boldsymbol{K}_{60},\ \boldsymbol{M}_1=\boldsymbol{M}_{73},\ M_2=\boldsymbol{M}_{74},$$

$$\boldsymbol{M}_3=\boldsymbol{M}_{75},\ \boldsymbol{M}_4=\boldsymbol{M}_{76},\ \boldsymbol{M}_5=\boldsymbol{M}_{77}.$$

Repeating the refinement steps in the previous section obtains the following correction factors: α_1=0.0682, α_2=−0.1117, β_1=0.0939, β_2=−0.2007, β_3=−0.0578, β_4=−0.0229, and β_5=−0.104. After model refining, the first three natural frequencies agree with those of the measured model well, and the MAC values also improve (Table 8).

For simplicity, only the case of 10 sensors is investigated (Fig.11). After the iteration procedure, the following correction factors are obtained: α_1=0.0693, α_2=−0.1153, β_1=0.093, β_2=−0.2084, β_3=−0.0595, β_4=−0.0258, and β_5=−0.0958. The first three natural frequencies and MAC values of the updated model are listed in Table 9. Results show that the updated model still agrees with the measured model well for both natural frequencies and mode shapes unlike in the model reduction case even though the sensors are limited. This finding may be due to the natures of the different schemes. Modal expansion is applied to the modal model, whereas model reduction is used for the spatial model. Thus, the resultant expression for the expanded mode shapes is simply an interpolation based on the mode shapes derived from the analytical model (Ewins, 2000). The correlation of the updated model with the measured model is significantly greater than that of the updated reduced model with the measured model.

Table 7 MAC values between expanded and analytical mode shapes

Mode	MAC				
	Measured	Guyan	Kidder's	SEREP	Full order
1	0.9424	0.8811	0.8811	0.9479	1
2	0.9256	0.6870	0.6869	0.9939	1
3	0.9850	0.9862	0.9862	1.0000	1

Table 8 Frequencies and MAC values for the updated model

Mode	Full order model		Updated model		Measured model
	Freq. (Hz)	MAC	Freq. (Hz)	MAC	Freq. (Hz)
1	10.896	0.9479	10.902	0.9532	10.902
2	11.019	0.9939	11.036	0.9977	11.036
3	14.392	1.0000	14.777	0.9999	14.777

Table 9 Frequencies and MAC values for the updated model (10 sensors)

Mode	Full order model		Updated model		Measured model
	Freq. (Hz)	MAC	Freq. (Hz)	MAC	Freq. (Hz)
1	10.896	0.9520	10.902	0.9568	10.902
2	11.019	0.9956	11.036	0.9961	11.036
3	14.392	0.9999	14.777	0.9999	14.777

4 Concluding Remarks

In modal testing, spatially incomplete measured information often occurs because of the limited number and locations of sensors. To solve the incompatibility of the order (the number of DOFs) of the models derived respectively from tests (measured models) and theoretical analysis (analytical models), the DOFs of analytical models are reduced by using model reduction methods or the measured DOFs are expanded by using modal expansion methods. In this paper, the developed model refinement scheme was extended to solve the combined model refinement and model updating problems. The scheme was applied in a physical model experiment of a jacket offshore platform. First, the first three modes of the physical model were identified from measured response data. Then, Guyan model reduction and SEREP were performed to reduce the full-order FE model and expand the measured mode shapes to obtain the initial refinement model, respectively. To avoid unfavorable conditions in solving the CMCM equations, seven updated elements were selected by modeling the error location and through sensitivity analysis of the updating parameters to the first three modes. After the model refinement procedure, the updated models could match the first three modes with those of the measured model well. Considering practical engineering requirements, two more sensor arrangements scenarios are also investigated. Numerical results of model reduction show that the mode shapes of the updated model hardly match the measured model perfectly. However, for the modal expansion case, the obtained updated model agrees with the measured model well in all scenarios.

Acknowledgements

This research was supported by the Major Program of the National Natural Science Foundation of China (No. 51490675), the National Natural Science Foundation of China (No. 51479183), and the Taishan Scholars Program of Shandong Province.

References

Doebling, S. W., Farrar, C. R., Prime, M. B., and Shevitz, D. W.,

1998. A review of damage identification methods that examine changes in dynamic properties. *The Shock and Vibration Digest*, **30** (2): 91-105.

Ewins, D. J., 2000. *Modal Testing: Theory, Practice and Application.* 2nd edition, Research Studies Press Ltd., Baldock Hertfordshire, England, 1-21, 349-359.

Friswell, M. I., and Mottershead, J. E., 1995. *Finite Element Model Updating In Structural Dynamics*. Kluwer Academic Publishers, Dordrecht, Netherlands, 56-77.

Guyan, R. J., 1965. Reduction of stiffness and mass matrices. *AIAA Journal*, **3** (2): 380.

Hu, S. L. J., Bao, X. X., and Li, H. J., 2010. Model order determination and noise removal for modal parameter estimation. *Mechanical Systems and Signal Processing*, **24** (6): 1605-1620.

Hu, S. L. J., Bao, X. X., and Li, H. J., 2012. Improved polyreference time domain method for modal identification using local or global noise removal techniques. *Science China Physics, Mechanics and Astronomy*, **55** (8): 1464-1474.

Hu, S. L. J., Li, H. J., and Wang, S. Q., 2007. Cross-model cross-mode method for model updating. *Mechanical Systems and Signal Processing*, **21** (4): 1690-1703.

Kidder, R. L., 1973. Reduction of structural frequency equations. *AIAA Journal*, **11** (6): 892.

Li, H. J., Zhang, M., and Hu, S. L. J., 2008. Refinement of reduced-models for dynamic systems. *Progress in Nature Science*, **18** (8): 993-997.

Liu, F. H., and Li, H. J., 2013. A two-step mode shape expansion method for offshore jacket structures with physical meaningful modeling errors. *Ocean Engineering*, **63**: 26-34.

Liu, F. S., 2011. Direct mode-shape expansion of a spatially incomplete measured mode by a hybrid-vector modification. *Journal of Sound and Vibration*, **330** (18-19): 4633-4645.

Liu, F. S., 2011. Direct mode-shape expansion of a spatially incomplete measured mode by a hybrid-vector modification. *Journal of Sound and Vibration*, **330** (18-19): 4633-4645.

Maia, N. M. M., Silva, J. M. M., He, J., Lieven, N., Lin, R. M., Skingle, G. W., To, W. M., and Urgueira, A. P. V., 1997. *Theoretical and Experimental Modal Analysis*. Research Studies Press Ltd., Taunton, Somerset, England, 193-199.

O'Callahan, J., Avitabile, P., and Riemer, R., 1989. System equivalent reduction expansion process (SEREP). *Seventh International Modal Analysis Conference*, Las Vegas, Nevada, 29-37.

Paz, M., 1984. Dynamic condensation. *AIAA Journal*, **22** (5): 724-727.

Peeters, B., 2000. System identification and damage detection in civil engineering. PhD thesis. Katholieke Universiteit Leuven.

Rade, D. A., and Lallement, G., 1998. A strategy for the enrichment of experimental data as applied to an inverse eigensensitivity-based FE model updating method. *Mechanical Systems and Signal Processing*, **12** (2): 293-307.

(Edited by Xie Jun)